Journal of
Synchrotron
Radiation

ISSN 0909-0495

Received 5 July 2007
Accepted 30 August 2007

Nitrogen *K*-edge XANES – an overview of reference compounds used to identify 'unknown' organic nitrogen in environmental samples

Peter Leinweber,[a]* Jens Kruse,[a] Fran L. Walley,[b] Adam Gillespie,[b] Kai-Uwe Eckhardt,[a] Robert I. R. Blyth[c] and Tom Regier[c]

[a]Institute for Land Use, University of Rostock, Justus von Liebig Weg 6, 18057 Rostock, Germany, [b]Department of Soil Science, University of Saskatchewan, Saskatoon, Canada S7N 5A8, and [c]Canadian Light Source Inc., University of Saskatchewan, Saskatoon, Canada S7N 0X4. E-mail: peter.leinweber@uni-rostock.de

The chemical nature of soil organic nitrogen (N) is still poorly understood and one-third to one-half of it is typically classified as 'unknown N'. Nitrogen *K*-edge XANES spectroscopy has been used to develop a systematic overview on spectral features of all major N functions in soil and environmental samples. The absolute calibration of the photon energy was completed using the $1s \rightarrow \pi^*$ transitions of pure gas-phase N_2. On this basis a library of spectral features is provided for mineral N, nitro N, amino acids, peptides, and substituted pyrroles, pyridines, imidazoles, pyrazoles, pyrazines, pyrimidines and purine bases. Although N XANES was previously considered 'non-destructive', effects of radiation damage were shown for two compound classes and an approach was proposed to minimize it. This new evidence is integrated into a proposal for the evaluation spectra from environmental samples with unknown composition. Thus a basis is laid to develop N *K*-edge XANES as a complementary standard research method to study the molecular composition and ecological functions of 'unknown N' in soil and the environment.

Keywords: soil nitrogen; heterocycles; soft X-ray spectroscopy; radiation damage; NEXAFS.

1. Introduction

Organic nitrogen (N) compounds in soils are both a source and sink for N in the global N cycle. The soil organic N pool provides the substrate for microbial formation of mineral N (NH_4 and NO_3) essential for agricultural production and likewise is the source of serious environmental pollution (*e.g.* NO_3 contamination of groundwater and emissions of N_2O, an important greenhouse gas). Despite its importance, the organic N pool contributing to N mineralization has not been adequately defined at the molecular level (Curtin & Wen, 1999) and the chemical nature of soil organic N remains poorly understood (Schulten & Schnitzer, 1998). Indeed, one-third to one-half of organic N in soil is typically classified as 'unknown N' (Stevenson, 1994) and the chemistry of this N fraction remains one of the most controversial soil chemistry issues in the literature. The controversy exists, and remains unresolved, largely because research has been hampered by the absence of definitive analytical methods (Stankiewicz, 1998).

To date, four different analytical approaches have been used to identify organic N fractions: (i) wet chemistry, which has included hydrolysis in 6N HCl, and wet-chemical fractionation into hydrolysable N, NH_3-N and unidentified N (Leinweber & Schulten, 1999), sometimes accomplished by the separation and quantification of individual amino acids in the hydrolyzate (Catroux & Schnitzer, 1987); (ii) Curie-point-pyrolysis gas chromatography/mass spectrometry (Cp Py-GC/MS) and pyrolysis-field ionization mass spectrometry (Py-FIMS), often applied complimentarily (Schulten *et al.*, 1997; Schulten & Schnitzer, 1998); (iii) ^{15}N nuclear magnetic resonance spectroscopy (^{15}N NMR) (Knicker *et al.*, 1993; Knicker, 2000); and (iv) X-ray spectroscopic methods such as X-ray photoelectron spectroscopy (Abe & Watanabe, 2004) and X-ray absorption near-edge structure (XANES) spectroscopy (Vairavamurthy & Wang, 2002; Jokic, Schulten *et al.*, 2004; Jokic, Cutler *et al.*, 2004; Zhuang *et al.*, 2006).

There is general agreement that proteinaceous materials constitute the majority of soil organic N (Schulten & Schnitzer, 1998; Stevenson & Cole, 1999; Knicker, 2000); however, opinions diverge regarding the proportions and chemical nature of non-proteinaceous N compounds. For example, using wet chemical fractionation, Leinweber & Schulten (1999) concluded that heterocyclic N compounds comprise about 25% of organic N in soil. Similarly, others have suggested that heterocyclic N accounts for about 35% of

organic N in soil on the basis of studies using GC/MS, Cp Py-GC/MS and Py-FIMS (Schulten *et al.*, 1997; Schulten & Schnitzer, 1998). These observations are consistent with the wide range of heterocyclic N compounds documented in plant materials (Pedras *et al.*, 2003; Somei & Yamada, 2004). However, Py-MS estimates have been criticized because heterocyclic N can form as an artifact of dissociation or rearrangement of the original structures during heating (Burdon, 2001; Vairavamurthy & Wang, 2002). This argument was supported by ^{15}N NMR studies that sometimes failed to detect heterocyclic N (Knicker, 2000; DiCosty *et al.*, 2003; Sjöberg *et al.*, 2004) or only detected it in soils affected by wildfires (Knicker *et al.*, 2005). However, others have suggested that ^{15}N NMR spectroscopy is simply too insensitive to detect some soil organic N compounds because of the low ^{15}N natural abundance (~0.37%) in soil (Vairavamurthy & Wang, 2002) and overlap of spectral features of pyrrole-, indole- and purine-N with those of peptide-, amide- and pyrimidinic N (Abe & Watanabe, 2004; Kelemen *et al.*, 2002).

Synchrotron-based XANES is a molecular-scale spectroscopy technique that yields electronic and structural information on the element of interest. An XANES spectrum is usually characterized by intense resonance features, arising from 1*s* electron transitions to unoccupied orbital and continuum levels and from multiple scattering of the emitted photoelectrons by the geometrical arrangement of neighbouring atoms around the absorbing atom. The energy position of the resonance features is related to the chemical environment of the absorber, such as oxidation state (Stöhr, 1992; Schulze & Bertsch, 1995; Fendorf & Sparks, 1996). In the early 1990s, XANES at the N *K*-edge was used to determine the chemical structure of organically bound N in fossil fuels such as petroleum asphaltenes (Mitra-Kirtley *et al.*, 1993). More recently, N *K*-edge XANES was successfully applied to characterize structures of N atoms in samples from biomaterials (*e.g.* Fujii *et al.*, 2003; Samuel *et al.*, 2006), interstellar matter (*e.g.* Feser *et al.*, 2003; Wirick *et al.*, 2004), material sciences (*e.g.* Watanabe *et al.*, 2002; Choi *et al.*, 2005) and carbon combustion technology (*e.g.* Xiao *et al.*, 2005). In the first application of N *K*-edge XANES spectroscopy to geomacromolecules in environmental samples, Vairavamurthy & Wang (2002) noted that heterocyclic N compounds constituted up to 30% of total N in chemically fractionated humic substances and sediments, and postulated that abiotic formation of heterocyclic N compounds may occur during early organic matter transformations. More recently, Jokic, Schulten *et al.* (2004) used N *K*-edge XANES to demonstrate a possible mechanism for abiotic formation of heterocyclic N. Jokic, Cutler *et al.* (2004) subsequently used N *K*-edge XANES to detect the presence of heterocyclic N compounds in chemically unaltered whole soil samples. These recent studies provide compelling evidence for heterocyclic N, and also demonstrate that synchrotron-based spectroscopy offers a powerful chemical and structural probe for the study of soil organic N in whole soils. Because XANES is based on electron excitation, the method is considered to be non-destructive as the structure of the molecules remains unchanged and N speciation is unaltered (Vairavamurthy & Wang, 2002). Moreover, N XANES detects all N present, and not just ^{15}N as with ^{15}N NMR. However, as for other sophisticated analytical-chemical methods, the quality of results obtained by N XANES will depend on technical details of facility and equipment, and choice of appropriate reference standard substances for comparison with spectra from samples of unknown chemical composition.

Vairavamurthy & Wang (2002), and subsequently Jokic, Schulten *et al.* (2004) and Jokic, Cutler *et al.* (2004), interpreted N *K*-edge XANES spectra of environmental samples of different origins on the basis of analyses of a limited set of reference compounds including 2,6-di-*p*-tolylpyridine, 6-hydroxyquinoline, quinoline 6-carboxylic acid and acridine (pyridines), pyridine 2,5-dicarboxylic acid, pyridoxal 5′-phosphate (oxidized pyridine derivatives), 4,6-dihydroxyl pyridine (pyridone), carbazole, poly(9-vinylcarbazole) (pyrrole), albumin, *N*-acetyl-D-glucosamine, glycine anhydride (amide/peptide) and 4-nitrophenyl acetic acid (nitro compound). However, considering the findings of gel-chromatography acetylation GC/MS and Py-MS (Schulten & Schnitzer, 1998), the N *K*-edge XANES spectra of reference compounds including imidazoles, pyrazoles, pyrazines and pyrimidines are essential as some of them are DNA/RNA building blocks, which were identified in soils (Anderson, 1961; Cortez & Schnitzer, 1979). Recent quantification of DNA in soils (Bürgmann *et al.*, 2001) supports the importance of these molecules for a complete picture of soil organic N. Therefore, our objective was to provide a systematic overview of the spectral features of all major N functions that potentially occur in soils and soil-related materials. Our strategic aim is to develop N *K*-edge XANES as a complementary standard research method in soil organic chemistry.

2. Experimental

The chemicals used as reference compounds were purchased from Sigma Aldrich, and the CAS (Chemical Abstracts Service) numbers are given in Table 1. All reference compounds were used without further purification. Powdered samples were applied to double-sided carbon tape (G3939, Plano GmbH, D-35578 Wetzlar, Germany) attached to a 10 mm-diameter stainless steel sample holder before insertion into the X-ray absorption chamber. To avoid problems associated with self-absorption, all reference compounds were spread as a very thin film onto the sample holder.

The N *K*-edge XANES spectra were measured on beamline 11ID-1 at the Canadian Light Source synchrotron. This beamline is equipped with a spherical-grating monochromator and is capable of providing 10^{11} photons s^{-1} at the N *K*-edge with a resolving power ($E/\Delta E$) better than 10000 with an exit slit setting of 5 µm (Regier *et al.*, 2006). For most measurements the exit slit was set at 50 µm. Only a few of the amino acids were measured using the 25 µm exit slit. The spectra were recorded in total fluorescence yield using a two-stage multichannel plate detector.

Table 1
Experimental energy positions of the main spectral features in the N *K*-edge spectra of various nitrogen compounds.

N group	N compound	CAS	Total N (mg g^{-1})	Peak 1	Peak 2	Peak 3	Peak 4	Peak 5	Peak 6
Mineral N	Ammonium phosphate, $(NH_4)_3PO_4$	7783-28-0	281.9	401.0	405.9				
	Ammonium nitrate, NH_4NO_3	6484-52-2	350.1	401.1	404.1	405.4			
	Ammonium sulfate, $(NH_4)_2SO_4$	7783-20-2	212.0	401.1	406.0				
	Potassium nitrate, KNO_3	7757-79-1	135.5	401.7	405.4	412.3			
	Calcium nitrate hydrate, $Ca(NO_3)_2$	35054-52-5	170.0	401.7	405.4	412.6			
Nitro groups	3-Nitrophthalic acid	603-11-2	66.3	399.4	401.1	403.8	413.8		
	4-Nitrophenyl acetate	830-03-5	77.3	403.9	413.7				
Amino acids	L-Arginine	74-79-3	321.7	399.0†	401.7	405.9			
	DL-Aspartic acid	617-45-8	105.3	406.2					
	L-Lysine	56-87-1	191.6	398.8†	400.8	402.2	405.6		
	D-Methionine	348-67-4	94.0	398.8†	406.8				
	L-Alanine	56-41-7	157.2	398.9†	401.1	405.9			
	L-Glutamic acid	56-86-0	95.2	398.9†	401.1	405.7			
	L-Threonine	72-19-5	117.6	398.8†	401.1	405.8			
	L-Valine	72-18-4	119.6	398.8†	406.1				
	L-Leucine	61-90-5	106.8	398.9†	405.9				
	L-Glutamine	56-85-9	191.7	398.9†	401.3	405.7			
	L-Serine	56-45-1	133.3	398.9†	401.1	405.9			
	L-Histidine	71-00-1	270.9	398.9†	400.0	401.6	406.6		
	L-Proline	147-85-3	121.7	398.9†	405.5				
Amines, amides	Albumin	9048-46-8	–	398.9†	399.9†	401.4	406.4		
	N-Acetyl-D-glucosamine	7512-17-6	63.3	399.0†	399.8†	401.4	406.3		
	Chitin	1398-61-4	–	399.0	401.5	405.6			
	D-Glucosamine hydrochloride	66-84-2	65.0	400.0	405.7				
	Sulfanilamide	63-74-1	162.7	398.5	406.0				
Five-ring heterocycles (1N)	Pyrrole-2-carboxylic acid	634-97-9	126.1	401.1	403.7	406.9			
	Carbazole	86-74-8	83.8	402.4	407.0				
	3-Indole-acetonitrile	771-51-7	179.4	398.6	399.9	402.2	407.3		
Six-ring heterocycles (1N)	6-Hydroxyquinoline	580-16-5	96.5	398.7	409.0				
	2,3-Pyridinedicarboxylic acid	89-00-9	83.8	398.7	399.8	407.6			
	4-Hydroxy-2-pyridone ('2,4-dihydroxypyridine')	626-03-9	126.1	401.0	405.1	408.1			
Five- and six-ring heterocycles (1N)	3-(Pyrrol-1-ylmethyl)-pyridine	80866-95-1	177.1	398.8	402.2	407.8			
Five-ring heterocycles (2N)	Imidazole-4-acetic acid, sodium salt	56368-58-2	189.2	400.0	401.8	406.9			
	L-β-Imidazolelactic acid	14403-45-3	179.6	400.0	401.7	406.9			
	4-Imidazoleacrylic acid	104-98-3	202.9	400.1	401.4	407.0			
	2-Methyl-4-nitro-1*H*-imidazole	696-23-1	330.7	399.1	399.9	402.2	403.9	407.3	
	3,5-Pyrazoledicarboxylic acid monohydrate	3112-31-0	160.9	400.0	401.5	406.9			
	1*H*-Pyrazole-1-carboxamidine hydrochloride	4023-02-3	382.3	399.8	400.6	402.3	404.4	406.7	
Six-ring heterocycles (2N)	Pyrazinecarboxylic acid	98-97-5	225.8	398.7	402.9	408.2			
	2,3-Pyrazinedicarboxylic acid	89-01-0	166.6	398.8	400.2	402.6	407.7		
	Pyrazinecarboxamide	98-96-4	341.4	398.7	400.0	402.6	408.2		
	2-Pyrimidinecarbonitrile	14080-23-0	399.8	398.8	400.0	401.9	402.6	404.5	408.6
	Cytosine	71-30-7	378.3	399.2	400.6	403.0	405.0	408.4	
	Uracil	66-22-8	250.0	401.1	402.2	405.3	407.0		
	Thymine	65-71-4	222.2	401.4	402.2	405.1	407.3		
	4,5,6-Triaminopyrimidine sulfate salt, hydrate	6640-23-9	290.4	399.6	401.0	406.6			
	Sulfadimethoxine	122-11-2	180.6	399.8	403.7	407.3			
Five- and six-ring heterocycles (2N)	Adenine	73-24-5	518.4	399.7	401.6	407.4			
	Adenosine 5′-diphosphate	58-64-0	164.0	399.9	401.4	407.6			
	Adenosine 5-monophosphate	61-19-8	201.7	399.5	401.1	407.0			
	Guanine	73-40-5	463.5	399.9	401.1	406.9			
	Deoxyribonucleic acid sodium salt	9007-49-2	–	399.4	401.6	406.9			
	Ribonucleic acid	63231-63-0	–	401.3	406.1				

† Probably due to radiation damage.

The absolute calibration of the photon energy was completed using the $1s \rightarrow \pi^*$ transitions of pure gas-phase N_2 and monitored over time using the same transition in 6-hydroxyquinoline, guanine, adenine and 2,3-pyrazinedicarboxylic acid. An absorption spectrum for N_2 was measured using a photoionization chamber mounted just upstream of the solid sample analysis chamber (Regier *et al.*, 2007). The well studied $1s \rightarrow \pi^*$ vibrational manifold has an energy of 400.8 eV for the $v = 0$ transition (Schwarzkopf *et al.*, 1999). The N *K*-edge XANES measurement of the above reference standards exhibit a sharp $1s \rightarrow \pi^*$ peak which was calibrated using the N_2 data. As the experiment took place over several different measurement periods, the beamline calibration could not be considered static, so one or more of the above reference standards was measured in two or more experimental runs and the energy calibration adjusted accordingly.

Data reduction was carried out using *Athena* (Version 0.8.05) (Ravel & Newville, 2005). The fluorescence data of at

least two scans were averaged and background corrected by a linear regression fit through the pre-edge region. Then all spectra were normalized to an edge jump of 1. The spectra presented were smoothed by interpolation with two iterations.

3. Results and discussion

3.1. Spectra of reference compounds

Figs. 1 to 11 show the stacked N *K*-edge XANES spectra of standard reference compounds arranged into groups with similar structural properties. All spectral features in the energy range 398.6 to 405 eV reflect $1s \rightarrow \pi^*$ transitions, and the broader spectral features at higher energies >405 eV reflect $1s \rightarrow \sigma^*$ transitions. The energy positions of the most intensive resonance in the normalized spectra are compiled in Table 1. The peak position and shape varied significantly for the different model compounds. Generally, this was more pronounced for the $1s \rightarrow \pi^*$ than for the $1s \rightarrow \sigma^*$ transitions. In our analysis, we compared spectra that we measured in common with those from other studies. In many cases, systematic shifts in peak positions are observed, indicating a difference in beamline calibration. Since previous studies have not indicated methods of photon energy calibration, we have applied these systematic shifts to compare with our own spectra as outlined in the sections below.

Fig. 1 shows the spectra of common mineral N compounds in soil. All ammonium compounds have a π^* resonance around 401 eV. The peak height of this resonance increased in the order $(NH_4)_2SO_4 > NH_4NO_3 > (NH_4)_3PO_4$. Additional high-resolution scans (boxed spectra on the left in Fig. 1) resolved the resonance at around 401 eV in a series of π^* resonances. The position and shape of these resonances were the same as reported for N_2 gas by Schwarzkopf *et al.* (1999). Therefore, we assign this peak to N_2 gas which was either trapped in the mineral N compounds or generated during X-ray exposure. The spectra of KNO_3 and $Ca(NO_3)_2$ had two sharp π^* resonances, one at 401.7 eV and the other at 405.4 eV. The first peak showed a small shoulder on the lower-energy side. This shoulder was more pronounced in the spectrum of $Ca(NO_3)_2$ than in the spectrum of KNO_3. This shoulder coincided with the assigned N_2 peak at 401 eV in the spectra of ammonium salts. In the high-resolution spectrum of KNO_3 some of the distinctive π^* resonance of N_2 gas were visible. Therefore the shoulder on the lower-energy side of the first π^* resonance at 401.7 eV can also be assigned to N_2 gas released during the measurement. However, the majority of this intensive resonance is difficult to assign. Since the nitrate-N has the diagnostic resonance at 405.4 eV in KNO_3 (Rodrigues *et al.*, 2007) and $Ca(NO_3)_2$ (Fig. 1), we interpret the resonance at 401.7 eV as a decomposition product. If this explanation is correct, formation of this nitrate decomposition product decreased in the order $KNO_3 > Ca(NO_3)_2 > NH_4NO_3$.

The high-energy peak of $(NH_4)_2SO_4$ and $(NH_4)_3PO_4$ at around 406 eV was assigned to the $1s \rightarrow \sigma^*$ transition. In the spectrum of NH_4NO_3 this transition was shifted by −0.6 eV. This can be explained by the overlap with the NO_3 peak at 405.4 eV. This indicates that peaks >405 eV can be assigned to $1s \rightarrow \sigma^*$ transitions preferably if the sample is free of NO_3-N. For NO_3-N the $1s \rightarrow \sigma^*$ transition appeared at around 412 eV in all three nitrate salts.

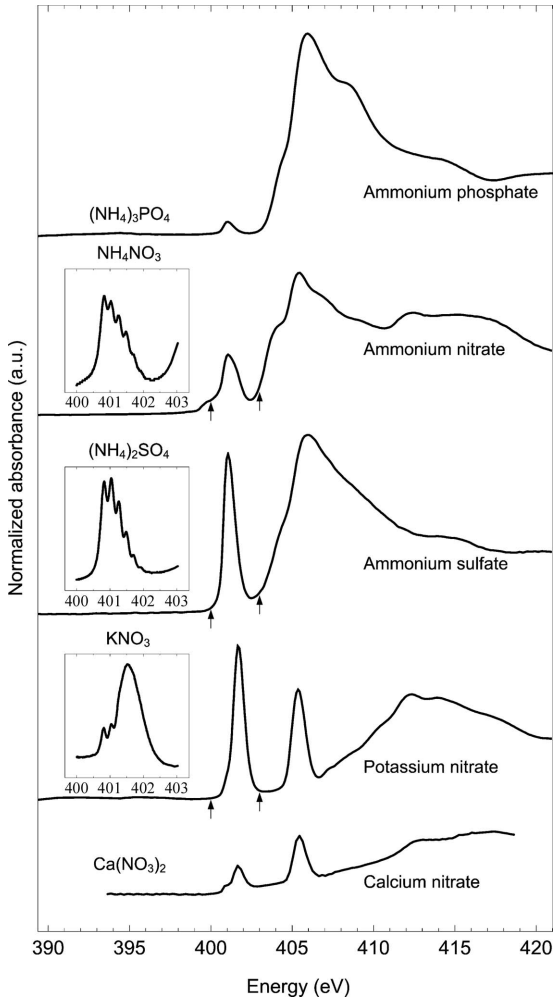

Figure 1
Nitrogen *K*-edge XANES spectra of mineral N compounds. Inset boxes show sections of high-resolution spectra acquired at 0.01 eV step size and 0.5 s dwell time between 401 and 403 eV as indicated by the arrows in the lower resolved spectra (0.1 eV step size and 1.0 s dwell time).

Spectra of compounds containing N only in a nitro group showed a sharp π^* peak at 403.8 to 403.9 eV and a broad high-energy peak around 413.7 eV (Fig. 2). This is explained by the higher positive charge at the N atom and, consequently, higher energy required for the $1s \rightarrow \pi^*$ transition. The energy position of the π^* resonance agreed with Pavlychev *et al.* (1995) who reported a peak at 403.3 eV for the nitro group. Furthermore, our spectroscopic features for the nitro group confirm previous data by Vairavamurthy & Wang (2002) if we shift their energy scale by −1.1 eV. Since Vairavamurthy & Wang (2002) did not report photon energy calibration, Jokic, Cutler *et al.* (2004) applied an energy shift of −1.2 eV, and subsequently obtained good agreement in the energy positions of spectral features.

Amino acids form the largest group among the reference compounds under study (Fig. 3). The majority of amino acid

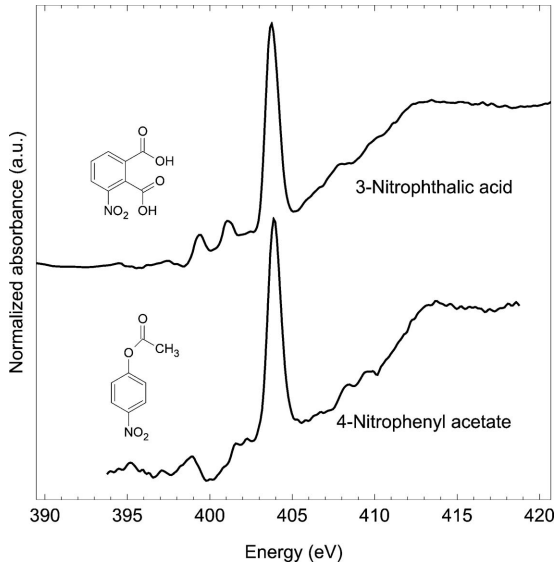

Figure 2
Nitrogen *K*-edge XANES spectra of nitro-N-containing compounds.

spectra were dominated by a relatively broad σ^* resonance peak at around 406 eV. All spectra showed a more or less pronounced peak at around 399 eV, followed by peaks or shoulders at around 401 eV, except for DL-aspartic acid, D-methionine, L-proline and L-histidine. The first three amino acids showed no spectral feature around 401 eV. The two sharp peaks at 400.0 and 401.6 eV in the L-histidine spectrum are assigned to the two N atoms in the heterocyclic molecule. The broad σ^* resonance peak at around 406 eV confirms previous data by Zubavichus *et al.* (2005) and Vairavamurthy & Wang (2002). Furthermore, the spectra of L-arginine and L-histidine also agreed with Zubavichus *et al.* (2005), who showed similar spectra with peaks at a slightly higher energy (+0.2 to –0.3 eV). The first peaks at around 399 eV in most spectra and at 401.1 in the spectrum of threonine were not seen by Zubavichus *et al.* (2005). This may be explained by the difference in photon flux incident on the sample, which might have led to radiation damage of our amino acids (Zubavichus *et al.*, 2005; 10^{11} photons s^{-1} at the spot size 1.2 mm × 0.5 mm *versus* 10^{11} photons s^{-1} in a 0.8 mm × 0.2 mm beam spot size). In a previous paper, Zubavichus, Zharnikov *et al.* (2004) discussed the sensitivity of amino acids to radiation damage. To check this, we compared the spectra obtained from the first scans with those of the second scans (Fig. 4). It appears that the peak at 398.8 eV (*a*) slightly increased in intensity and a new peak (*b*) became obvious at 400 eV. Furthermore, the shoulder at 401.6 eV (*c*) in the D-methionine spectrum became more pronounced towards a broad peak. The spectrum of D-arginine showed no difference to that of L-arginine (Fig. 3, Table 1). The sharp peak (*c*), assigned to a π^* transition of the guanidine structure (Zubavichus *et al.*, 2005), became less intense and broader. We explain these transformations in the spectra as chemical reactions in the sample under the impact of X-rays. Bozack *et al.* (1994) and Zubavichus, Zharnikov *et al.* (2004) described deamination and decarboxylation as

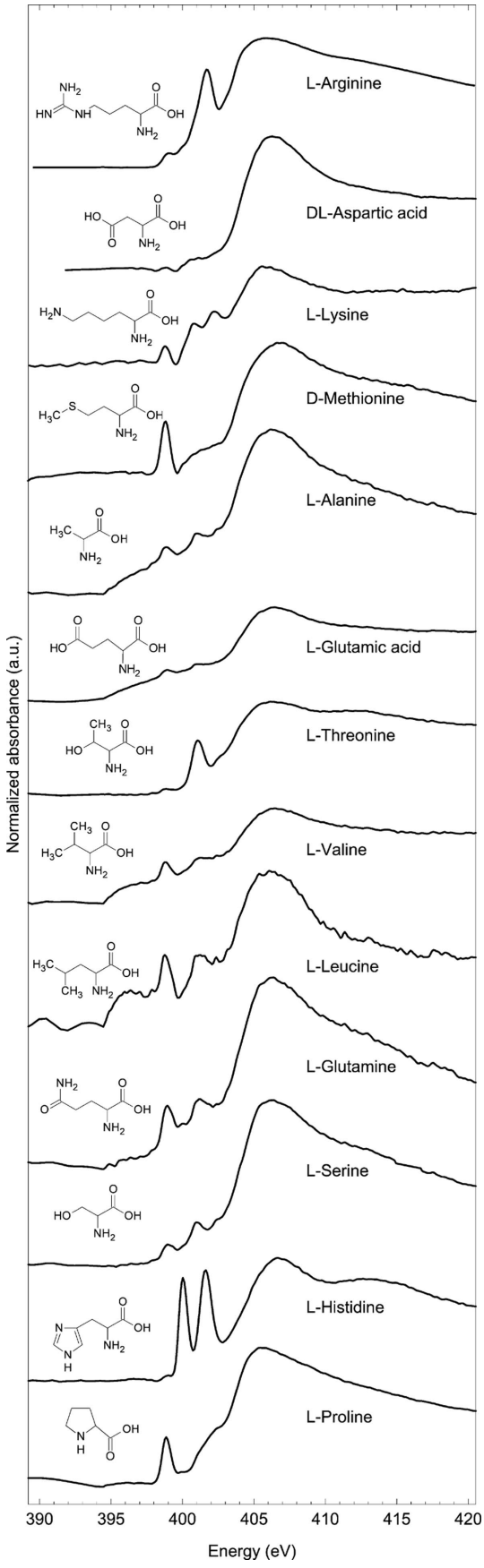

Figure 3
Nitrogen *K*-edge XANES spectra of amino acids.

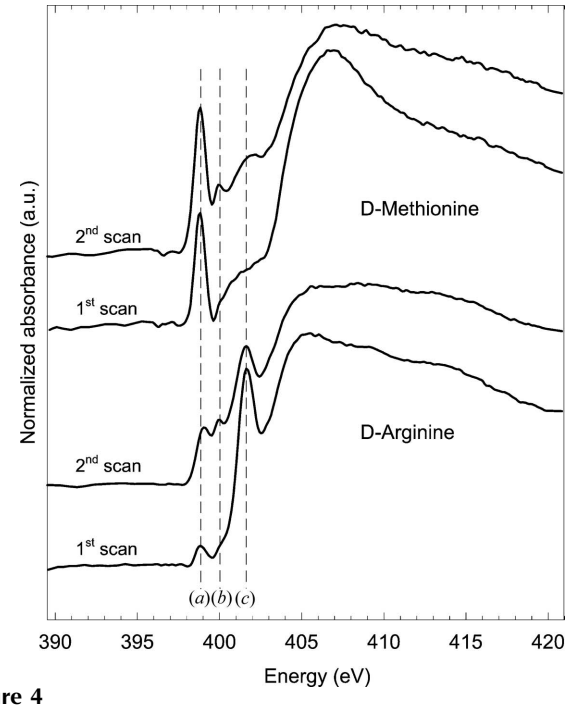

Figure 4
Nitrogen *K*-edge XANES spectra of amino acids: comparison of spectra merged from two first and second scans recorded at two different spots showing stability and damage of compounds under the beam impact.

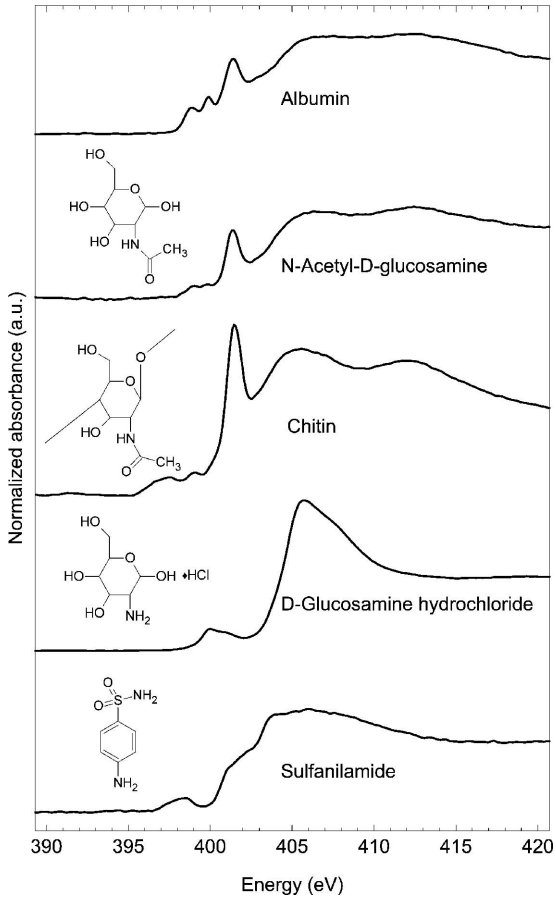

Figure 5
Nitrogen *K*-edge XANES spectra of amines and amides.

possible pathways for the decomposition of amino acids under the impact of soft X-rays. Zubavichus, Fuchs *et al.* (2004) found a series of new peaks in the range 399 to 403 eV after 4 to 14 min X-ray impact to cysteine. The peaks (*a*), (*b*) and (*c*) (D-methionine) and (*a*) and (*b*) (D-arginine) in Fig. 4, not observed in the spectra of Zubavichus *et al.* (2005), suggest that such decomposition reactions may have already occurred during our first scans.

The spectra of amide and amine compounds showed distinct π^* resonances around 401.4 eV (Fig. 5). This agrees well with Mitra-Kirtley *et al.* (1992) and Vairavamurthy & Wang (2002) (after calibration adjustments) and is explained by the π-electron cloud of the C═O bond closely coupled with the N. However, in contrast to Mitra-Kirtley *et al.* (1992) and Vairavamurthy & Wang (2002), our spectra of albumin and *N*-acetyl-D-glucosamine showed two low-energy resonances at around 399 eV and 399.9 eV. These resonances were more pronounced in the albumin than in the *N*-acetyl-D-glucosamine spectrum. Whereas both resonances were apparent in the first scan of albumin, these resonances were smaller in the first as compared with the second scans of *N*-acetyl-D-glucosamine (data not shown). Given the discrepancies between our results and those previously reported, together with observed spectral changes with subsequent scans, it is suggested that these resonances reflect N species formed by the impact of X-rays. It is possible that radiation damaged the amino acid polymer comprising albumin in a manner similar to that of pure amino acids. We conclude that the low-energy resonance at 398.9 eV in the albumin spectrum is due to X-ray decomposition whereas the second low-energy resonance at 399.9 eV can be attributed to both decomposition products and the first $1s \rightarrow \pi^*$ transition of L-histidine, which is an important constituent of albumin.

In the spectrum of chitin, a polymer of *N*-acetyl-D-glucosamine, the major peak occurred at 401.5 eV, and was more pronounced than in the monomer. This peak was missing in the spectra of D-glucosamine hydrochloride and sulfanilamide. These two compounds showed a broad low-intensity spectral feature around 400 eV (D-glucosamine hydrochloride) and 398.5 eV (sulfanilamide) and the broad spectral features of $1s \rightarrow \sigma^*$ transitions in the range 405.5 to 406.4 eV.

Pyrrole-2-carboxylic acid showed a distinct π^* peak at 401.1 eV, carbazole a broader peak at 402.4 eV, 4-hydroxy-2-pyridone a relatively narrow peak at 401 eV, and 3-indoleacetonitrile a broad but less intensive peak at 402.2 eV (Fig. 6). We assign these spectral features to the N atom in the pyrrole and pyridone structure. The energy positions of the π^* resonances of our pyrrole derivatives varied by approximately 1.3 eV. This is in agreement with others who also found that π^* peak energy positions varied up to +0.5 to −1 eV for different pyrrole derivatives (Mitra-Kirtley *et al.*, 1993; Mullins *et al.*, 1993; Henning *et al.*, 1996; Bach *et al.*, 1997; Vairavamurthy & Wang, 2002). This divergence can be explained by differences in the chemical structures of these compounds. Our carbazole spectrum confirms previous data by Mullins *et al.* (1993) and Mitra-Kirtley *et al.* (1993) if we shift their energy scales by −1.1 eV and −0.9 eV, respectively. The resonance at

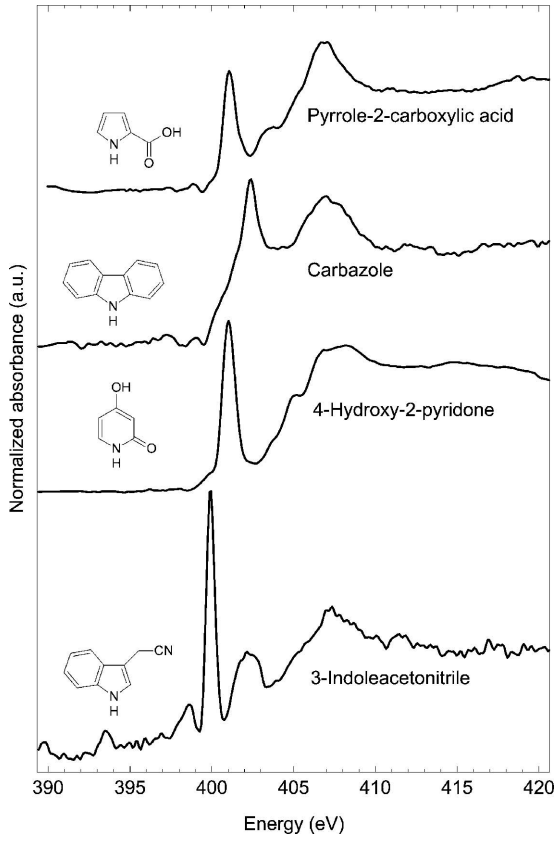

Figure 6
Nitrogen *K*-edge XANES spectra of five-ring heterocycles.

401 eV in the spectrum of 4-hydroxy-2-pyridone agreed with Vairavamurthy & Wang (2002) who called this substance 4,6-dihydroxypyridine. The designation as a pyridine can be misleading in this respect, because solid 2,4-dihydroxypyridine (synonym '3-deazaurazil') is stable in the tautomeric form 4-hydroxy-2-pyridone (Wilson, 1994). Pyridones generally had π^* resonances at 400.7 $\pm$ 0.2 eV (Mitra-Kirtley *et al.*, 1993; Vairavamurthy & Wang, 2002). The N in the pyridone structure is pyrrole-type as discussed below in more detail.

The spectrum of 3-indoleacetonitrile was largely dominated by another $1s \rightarrow \pi^*$ resonance at 399.9 eV. In agreement with previous studies of other nitrile compounds (Hitchcock *et al.*, 1989; Apen *et al.*, 1993; Carniato *et al.*, 2005; Ray *et al.*, 2005), we assign this peak to the nitrile structure. Since the nitrile bond has predominantly π character, an intensive peak is expected in the π^* region. This is also confirmed by nitrile in the spectrum for 2-pyrimidinecarbonitrile (see below). For all pyrrole derivatives the $1s \rightarrow \sigma^*$ transition was observed as a broad feature at around 407 eV.

The 6-hydroxyquinoline and 2,3-pyridinedicarboxylic acid spectra both showed $1s \rightarrow \pi^*$ resonances at similar energy position of 398.7 eV and 398.8 eV, respectively (Fig. 7), despite their different chemical structures. This energy position is in agreement with previous studies of other pyridine derivatives (Mitra-Kirtley *et al.*, 1992, 1993; Kelemen *et al.*, 1994; Vairavamurthy & Wang, 2002). All pyridine analogues showed a broad feature in the range 407.5 to 409 eV.

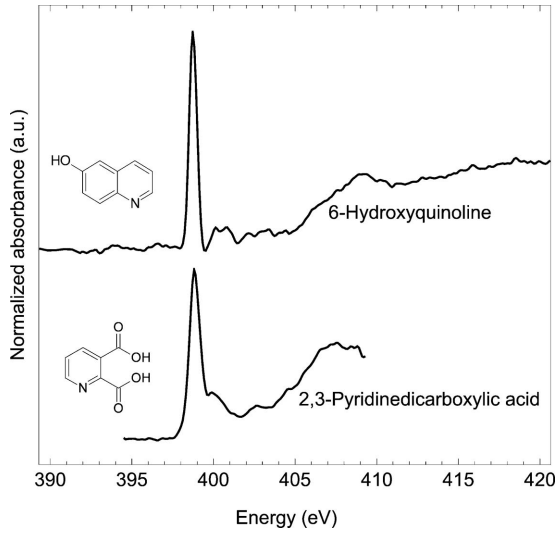

Figure 7
Nitrogen *K*-edge XANES spectra of 6-hydroxyquinoline and 2,3-pyridinedicarboxylic acid.

Fig. 8 compares the spectrum of 3-(pyrrol-1-ylmethyl) pyridine, which contains both a pyridine and a pyrrole structure, with the spectra of carbazole (pyrrole) and 2,3-pyridinedicarboxylic acid (pyridine). The spectrum of 3-(pyrrol-1-ylmethyl) pyridine showed two distinct and clearly separated π^* resonance features at 398.8 eV and 402.2 eV, respectively. The position of the lower-energy feature matches well with the π^* resonance of the pyridine derivative 2,3-pyridinedicarboxylic acid. The feature at 402.2 eV matches well with the π^* resonance of the pyrrole derivative carbazole or with pure pyrrole in the gas phase (Hennig *et al.*, 1996). Therefore, we assign the first π^* resonance in the spectrum of 3-(pyrrol-1-ylmethyl) pyridine to pyridinic N and the second higher-

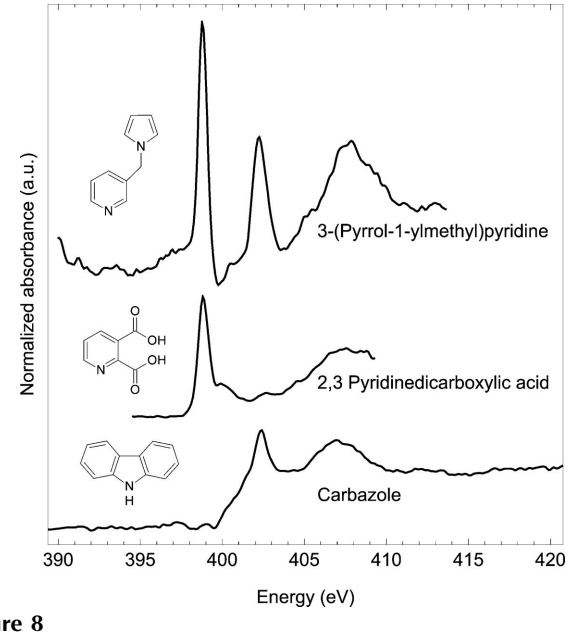

Figure 8
Nitrogen *K*-edge XANES spectra of a five- and six-membered heterocyclic compound compared with 2,3-pyridinedicarboxylic acid and carbazole.

energy π^* resonance to pyrrolic N. The difference in the energy position of the $1s \rightarrow \pi^*$ transition between pyridinic and pyrrolic N results from the difference in the effective nuclear charge of the absorbing N atom. It is known that the energy position of the π^* transition increases with increasing effective nuclear charge or decreasing electron density on the absorbing atom. The N atom in the pyridine structure has its lone pair unshared in the sp^2 orbital. The N atom in the pyrrole structure has the lone pair in the pz orbital, which is involved in the π cloud of the aromatic system. Therefore, pyrrole carries a lower electron density and consequently the π^* resonance is at a higher energy position.

All reference compounds having an imidazole structure showed at least two resonances, one around 400 eV and the other in the range 401.4 to 402.3 eV (Fig. 9). The imidazole structure contains two N atoms, which differ in the orbital description of the lone pair. Therefore, we assign the first resonance to the $1s \rightarrow \pi^*$ transition of the pyridinic and the second to the $1s \rightarrow \pi^*$ transition of the pyrrolic N. This assignment agrees with Apen *et al.* (1993) who measured imidazole in the solid and gas phase, and with Mitra-Kirtley *et al.* (1993) who described these two resonances in a 2-methylbenzimidazole spectrum. In the spectra of imidazole-4-acetic acid sodium salt and L-β-imidazolelactic acid the energy positions of both π^* resonances were almost identical. The same resonances were observed in the L-histidine spectrum in Fig. 3. For imidazole-4-acetic acid the first π^* resonance was slightly higher than the second resonance. For L-β-imidazolelactic acid (Fig. 9) and L-histidine (Fig. 3) the second resonance was higher in intensity than the first one. This difference in peak intensity was much more pronounced in the spectrum of 4-imidazoleacrylic acid. In this spectrum the peak for pyridinic N was reduced and formed a shoulder, and the peak for pyrrolic N appeared at 401.4 eV which is the lower end of the above range. The spectrum of 2-methyl-4-nitroimidazole was more complicated. We assign the peak at 399.9 eV to pyridinic N, the lower peak at 402.2 eV to pyrrolic N and the third peak at 403.9 eV to N of the nitro group. The assignment of the nitro-N agrees with the spectra in Fig. 2. 3.5-Pyrazoledicarboxylic acid monohydrate also exhibited two π^* resonances of pyridinic (400 eV) and pyrrolic N (401.5 eV). This agrees with the above imidazole spectra and is interpreted by the similarity in electronic structure. In the spectrum of 1-*H*-pyrazole-1-carboxamidine the peaks at 399.8 eV and 402.3 are assigned to pyridinic and pyrrolic N, respectively. The peaks were slightly shifted if compared with the above ranges for pyridinic and pyrrolic N in the imidazole and pyrazole structures. This shift, as well as the two other spectral features at 400.6 and 404.4 eV, is probably due to the amidine structure. The spectral features of $1s \rightarrow \sigma^*$ transitions were in the range 406.7 to 407.3 eV.

All spectra of the differently substituted pyrazines showed one sharp intensive peak at 398.7 to 398.8 eV (Fig. 10). This is explained by the cumulative effect of $1s \rightarrow \pi^*$ transitions of the two pyridinic N atoms. Less intensive small features at 400 to 400.2 eV and 402.6 to 402.9 eV seem to vary with substitution but cannot yet be assigned in detail. The pyrimidine

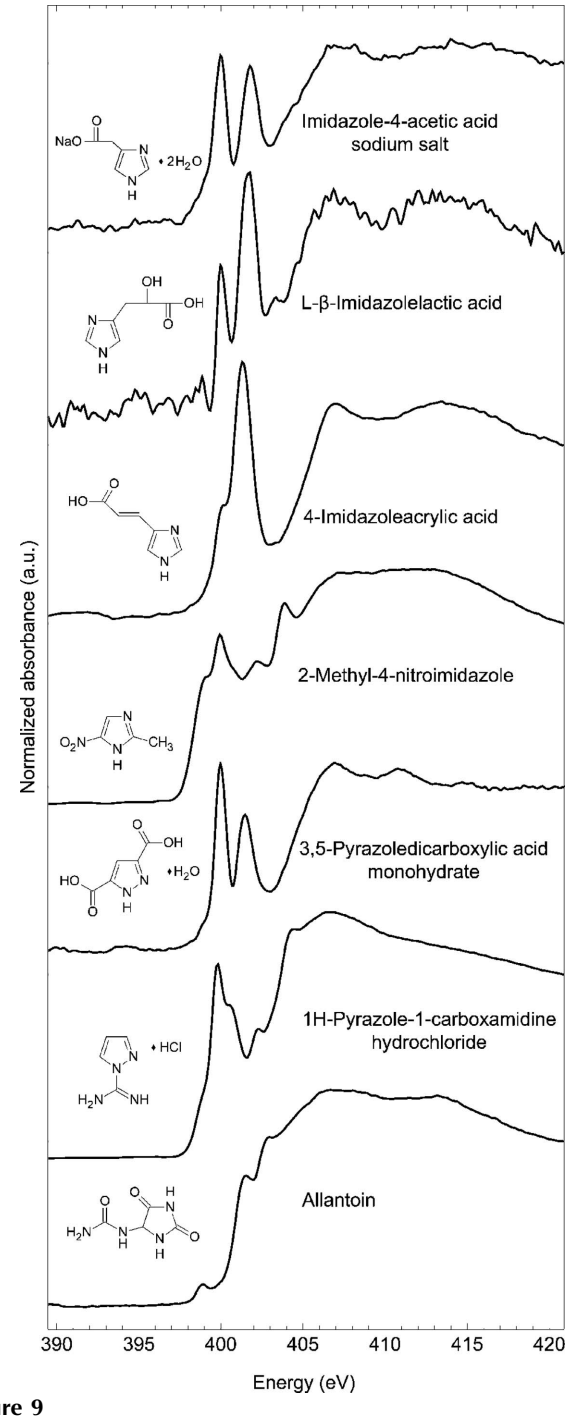

Figure 9
Nitrogen *K*-edge XANES spectra of five-ring heterocycles with at least two N atoms.

example 2-pyrimidinecarbonitrile also showed the intensive major peak at 398.8 eV because of the two pyridinic N atoms. In this spectrum the second peak at 400 eV is assigned to nitrile-N, in agreement with the nitrile peak in the spectrum of 3-indole-acetonitrile (Fig. 6). The σ^* resonances were relatively uniform in the range 407.7 to 408.2 eV.

The spectra of O-substituted pyrimidines cytosine, uracil and thymine showed π^* resonances at 399.2, 400.6 and 403 eV (cytosine), 401.1 to 401.4 eV and 402.2 eV (uracil and

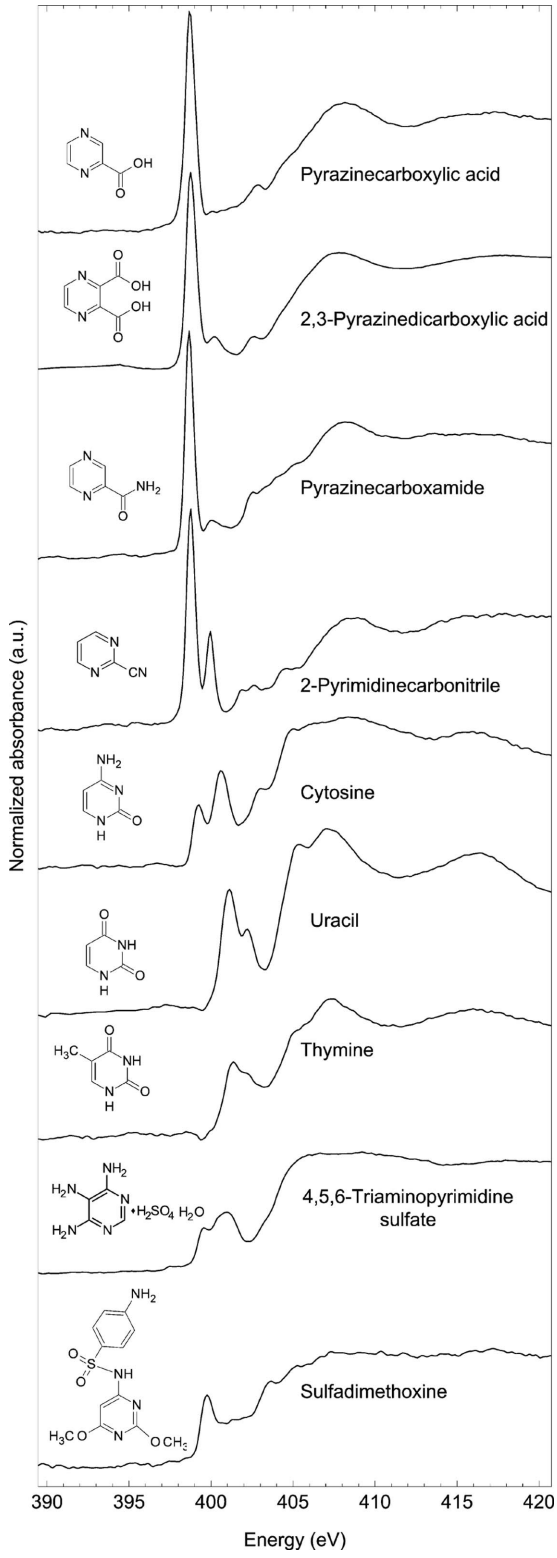

Figure 10
Nitrogen *K*-edge XANES spectra of six-ring heterocycles with at least two N atoms.

thymine). The double peak of the cytosine spectrum indicated pyridinic N (399.2 eV) and pyrrolic N (400.6 eV). The first peak was not observed in the spectra of uracil and thymine because they contain two pyrrolic N atoms. Comparison of the spectra of pyrimidines with, and without increasing O-substitution showed shifts of the π^* resonances towards a higher-energy position. This was true for the comparison of pyridinic N in 2-pyrimidinecarbonitrile and cytosine (+0.4 eV), and of pyrrolic N in cytosine compared with uracil and thymine (+0.5 eV). Obviously the O-substitution affected the two pyrrolic N atoms differently, which was reflected by the double peak in the uracil and the shoulder in the thymine spectrum. The methyl group in the spectrum of thymine did not alter the energy position of the π^* resonances but modified the shape of the spectrum. The spectra of pyrimidine bases showed several structural features in the σ^* resonance region. In general, these three spectra agreed well with Mitra-Kirtley *et al.* (1992) if we apply an energy shift of -1.4 eV. Furthermore, the spectra of cytosine and thymine (first peak only) agreed well with Samuel *et al.* (2006) if we apply an energy shift of 0.2 eV ($\pi1^*$) and +0.4 eV ($\pi2^*$) to their spectra.

The π^* resonances in the spectra of 4,5,6-triaminopyrimidinesulphate (399.6 eV) and sulfadimethoxine (399.8 eV) are slightly higher than in the above pyrazine and pyrimidine spectra.

The spectra of three compounds containing the purine structure all showed two π^* resonances in the range 399.5 to 399.9 eV, and 401.1 to 401.6 eV (Fig. 11). The first peaks were always more intensive than the second peaks. This is explained by the ratio of pyridinic N to pyrrolic N of 4:1. In the spectrum of guanine the larger proportion of pyrrolic N was reflected by an increased intensity of the second peak. The exocyclic O-substitution at the purine ring structure resulted in shifts towards higher energy of the pyridinic N (+0.2 eV) and pyrrolic N (+0.6 eV) peaks. The spectral features of $1s \rightarrow \sigma^*$ transitions were in the range 407 to 407.6 eV. Again the spectra of adenine and guanine agreed with Mitra-Kirtley *et al.* (1992) provided an energy shift of -1.4 eV is applied, and with Samuel *et al.* (2006) provided an energy shift of +0.4 eV is applied.

The spectrum of DNA showed peaks at 399.4 and 401.6 eV, confirming DNA spectra published by Mitra-Kirtley *et al.* (1992) and Fujii *et al.* (2003). Since the above pyrimidines and purine structures are the N-containing building blocks of DNA, the peaks are assigned to pyridinic N and pyrrolic N. Surprisingly, the spectrum of RNA showed only one π^* resonance at 401.3 eV. To the best of our knowledge, spectra of RNA have not been published before. The RNA differs from DNA in the sugar (ribose instead of desoxyribose), nucleobases (uracil instead of thymine) and the single-stranded conformation. Mitra-Kirtley *et al.* (1992) have shown that the glycosidic C—N linkage had an influence on the N *K*-edge XANES spectra of cytosine, uracil and guanine. More recently, Samuel *et al.* (2006) reported that addition of the DNA sugar and phosphate components resulted in noticeable, unexpected and still unexplained shifts of the π^* resonances such as the appearance and disappearance of resolved doublet π^*-peaks. Therefore, it can be hypothesized that the modification in the nucleobase and sugar possibly explains the completely different RNA spectrum. However, these preliminary results must be confirmed and RNA building blocks

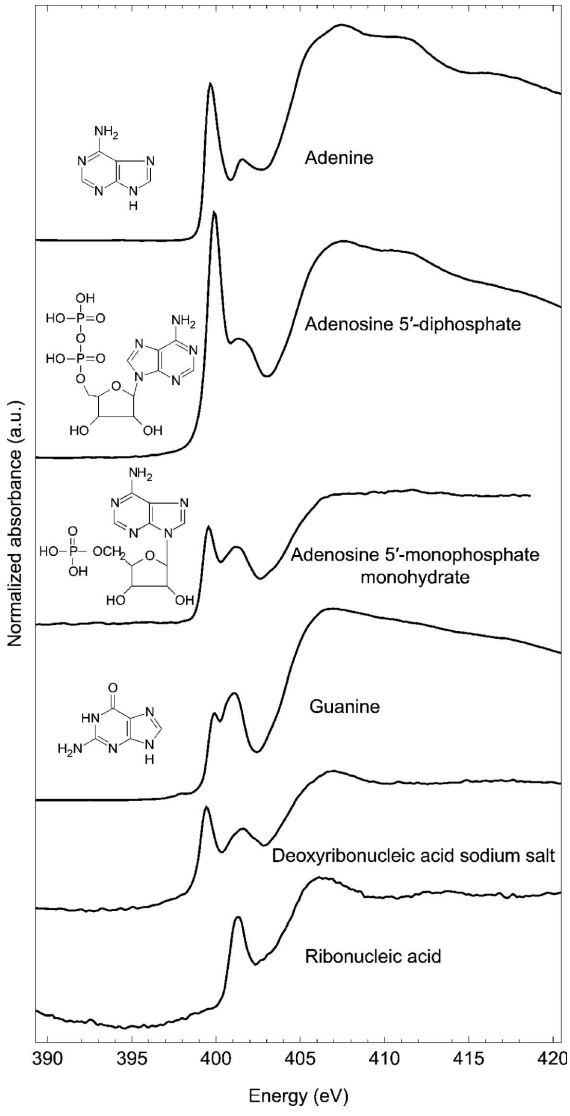

Figure 11
Nitrogen *K*-edge XANES spectra of five-ring and six-ring heterocycles which are ADP-, ATP-, RNA- and DNA-building blocks.

systematically studied in detail as recently shown for DNA (Samuel *et al.*, 2006).

For the evaluation of N *K*-edge XANES spectra from samples with unknown composition, the following points become crucial for the compilation of the present spectra and comparison with literature data.

(i) The π^* resonances at lowest energy (398.7 to 400 eV) can be assigned to pyridinic N in pyridines, imidazoles, pyrazoles, pyrazines, pyrimidines, cytosine and purine structures. Around 400 eV the π^* resonances of pyridinic N in pyrazoles and purine structures can interfere with those of nitrile N. Nitriles have been found in soil organic matter, and it was hypothesized that long-chain alkyl nitriles are soil specific (Schulten & Schnitzer, 1997; Leinweber & Schulten, 1998). Another relevant interference may originate from radiation damage products of amino acids, and labile peptides which showed up with peaks at 398.9 and 399.9 eV.

(ii) Pyrrolic N in pyrroles, imidazoles, pyrazoles, pyrimidines and purine structures showed the π^* resonance in the range 400.6 to 402.3 eV. Since this range was wider than previously reported by Mitra-Kirtley *et al.* (1993), Mullins *et al.* (1993), Hennig *et al.* (1996), Bach *et al.* (1997) and Vairavamurthy & Wang (2002), the present data confirm that pyrrolic N can clearly be differentiated from pyridinic N but may interfere with amide N.

(iii) Three spectra of different amides indicated 401.4 eV as the characteristic energy position of the amide N–π^* resonance. This overlaps with the energy range found for pyrrolic N. Furthermore, the N_2 gas peak (401 eV), unexpectedly released from mineral N, and a NO_3 peak at 401.6 eV also interfered with pyrrolic N and amide N. However, since mineral N generally constitutes less than 1% of total N in arable soils, this interference is likely not to be relevant for the interpretation of N *K*-edge XANES of soil samples. It would be relevant, for instance, for the interpretation of N *K*-edge XANES of soil solutions or leachates that contain proportionately more mineral N.

(iv) Accordingly, broad π^* resonance peaks at >400 eV may originate from amide N and pyrrolic N. The present data and the cited references showed a wide range of π^* resonances for pyrrolic N. Therefore it seems difficult to resolve such broad peaks without complementary information on the abundance of pyrrolic N compounds and amides in the sample. Since amino acids and amides were shown to be susceptible to radiation damage, we deemed it essential to test whether radiation damage is likely to occur for soils and related samples.

3.2. Does radiation damage affect the evaluation of spectra from soil samples?

Fig. 12 shows that the first scan and second scan at two different spots of a Melfort clay sample differed. The peak (*a*) around 398.9 eV was unchanged. In both of the second scans a shoulder appeared at around 400 eV (*b*) and a peak at 401.5 eV (*c*) seemed to be slightly lower in intensity. The position of this shoulder agreed with a new peak observed at 400 eV in the second scan of D-methionine and D-arginine in Fig. 4. Since the smaller peak (*c*) agreed in energy position with the characteristic π^* resonance of peptides (Fig. 5), it is likely that peptides and amino acids in the soil clay were decomposed under the beam impact. Radiation damage of amino acids observed by Zubavichus, Fuchs *et al.* (2004) was attributed to the formation of imino (C=NH) and nitrile (C≡N) derivatives. This was largely derived from combinations of C 1*s*, O 1*s* and N 1*s* XPS (X-ray photoelectron spectroscopy) spectra and electron impact-ionization mass spectrometry. The nitrile function in our spectra also had a π^* resonance at 399.9 eV (Figs. 6 and 10). Therefore, it is possible that nitriles were formed by radiation damage of peptides and amino acids in our samples although the formation of other N functions cannot be excluded. This partly disagrees with Vairavamurthy & Wang (2002) who concluded that X-ray analysis did not alter their sample spectra; however, their

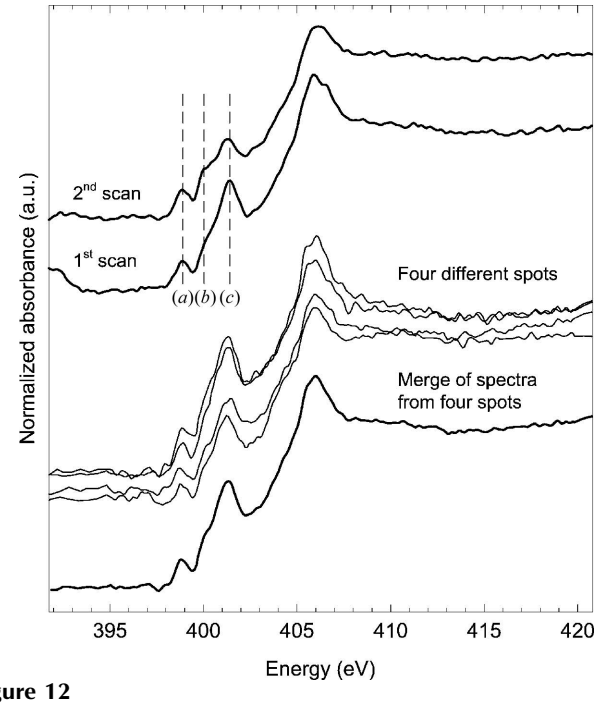

Figure 12
Nitrogen *K*-edge XANES spectra of a Melfort soil clay sample: comparison of spectra merged from two first and second scans recorded at two different spots (upper) and single scans recorded at four different spots and the corresponding merged spectrum.

experimental approach to studying radiation damage and explanation of Fig. 3 remained unclear. Cherezov *et al.* (2002) reported damage of soft condensed biomaterials such as lipids and membranes in bright X-ray synchrotron radiation. To avoid over-exposure they proposed to continuously move the sample during a measurement.

Movement of the Melfort clay sample after each scan and recording the spectra at four different spots avoided radiation damage owing to shorter exposure time (Fig. 12, lower). There were no differences in peak positions, and the merged spectrum agreed with the first scans of a separate sample of the Melfort coarse clay. Lower signal-to-noise ratios for the four individual scans pointed to the importance of scan replications, which should be recorded at different spots in a homogeneous sample. In this way, possible effects of radiation damage on the evaluation of spectra from soil samples can be minimized although we cannot exclude the possibility that the X-ray radiation during the first scan damaged compounds in the sample.

4. Conclusions

Identification of organic N compounds in soil and environmental samples remains an important challenge for soil and environmental scientists. Much of the current controversy regarding soil organic N relates to methodological constraints and limitations that have hampered efforts to unequivocally resolve its molecular nature. We have presented a systematic overview of the spectral features of all major N functions likely to occur in soils and soil-related environmental materials. This study provides a more comprehensive library of spectral features than previously reported. To the best of our knowledge, this is the first time that N *K*-edge XANES spectra of imidazoles, pyrazoles and purine structures have been reported and discussed in the context of naturally occurring organic N in soils. Since shifts in the peak position according to the electronic structure of N atoms in various molecules were more pronounced for the $1s \rightarrow \pi^*$ than for the $1s \rightarrow \sigma^*$ transitions, it is suggested that the diagnostic value of a spectral feature is greater for the π^* than for the σ^* region in the XANES spectra. At this time, N *K*-edge XANES can be employed to reliably distinguish two π^*-regions in spectra of unknown environmental samples: $\leq$400 eV (pyridinic N and some nitrile N) and >400 eV (amide N, nitro N and pyrrolic N). A quantitative estimate of the proportions of amide N and pyrrolic N requires a separate determination of one of the compounds, which remains a challenge for forthcoming studies. Furthermore, spiking experiments with multiple mixtures are necessary to evaluate to what extent pyridinic N and nitrile N can be distinguished in the low-energy range, and amide N and pyrrolic N in the higher-energy range. Radiation damage was observed for individual amino acids, amides and to some extent also for organic matter in a soil clay sample. Data suggest that radiation damage can be largely avoided by moving the sample holder after each scan. Given the subtle variations in spectral features, even for compounds sharing very similar structures, it is unlikely that the current N *K*-edge XANES can be used exclusively to quantitatively determine the chemical composition of an environmental sample. However, used in conjunction with existing complementary soil chemical analyses, N *K*-edge XANES can be developed as a powerful tool for elucidating the nature of 'unknown soil N'.

The N *K*-edge XANES measurements were performed at the Canadian Light Source, which is supported by NSERC, NRC, CIHR and the University of Saskatchewan. This work was supported by a travel grant of the German Academic Exchange Service (D/05/50492). We thank Professor M. S. C. Pedras, Department of Chemistry, University of Saskatchewan, for providing some of the reference compounds. Thanks also to two anonymous referees for helpful comments which improved the manuscript.

References

Abe, T. & Watanabe, A. (2004). *Soil Sci.* **169**, 35–43.
Anderson, G. (1961). *Soil Sci.* **91**, 156–161.
Apen, E., Hitchcock, A. P. & Gland, J. E. (1993). *J. Phys. Chem.* **97**, 6859–6866.
Bach, A., Beyer, L., Hennig, C., Hallmeier, K. H. & Sieler, J. (1997). *Chem. Mon.* **128**, 217–224.
Bozack, M. J., Zhou, Y. & Worley, S. D. (1994). *J. Chem. Phys.* **100**, 8392–8398.
Burdon, J. (2001). *Soil Sci.* **166**, 752–769.
Bürgmann, H., Pesaro, M., Widmer, F. & Zeye, J. (2001). *J. Microbiol. Methods*, **45**, 7–20.
Carniato, S., Taïeb, R., Kukk, E., Luo, Y. & Brena, B. (2005). *J. Chem. Phys.* **123**, 214301.

Catroux, G. & Schnitzer, M. (1987). *Soil Sci. Soc. Am. J.* **51**, 1200–1207.
Cherezov, V., Riedl, K. M. & Caffrey, M. (2002). *J. Synchrotron Rad.* **9**, 333–341.
Choi, C. H., Park, J. & Kim, B. (2005). *J. Phys. Chem. B*, **109**, 4333–4340.
Cortez, J. & Schnitzer, M. (1979). *Soil Sci. Soc. Am. J.* **43**, 958–961.
Curtin, D. & Wen, G. (1999). *Soil Sci. Soc. Am. J.* **63**, 410–415.
DiCosty, R. J., Weliky, D. P., Anderson, S. J. & Paul, E. A. (2003). *Org. Geochem.* **34**, 1635–1650.
Fendorf, S. E. & Sparks, D. L. (1996). *Methods of Soil Analysis: Chemical Methods*, edited by D. L. Sparks, pp. 377–416, *Soil Science Society of America Book Series 5.* Madison, WI: Soil Science Society of America.
Feser, M., Wirick, S., Flynn, G. J. & Keller, L. P. (2003). *34th Lunar and Planetary Science Conference*, 17–21 March 2003, Texas, USA.
Fujii, K., Akamatsu, K., Muramatsu, Y. & Yokoya, A. (2003). *Nucl. Instrum. Methods Phys. Res. B*, **199**, 249–254.
Hennig, C., Hallmeier, K. H., Bach, A., Bender, S., Franke, R., Hormes, J. & Szargan, R. (1996). *Spectrochim. Acta A*, **52**, 1079–1083.
Hitchcock, A. P., Tronc, M. & Modelli, A. (1989). *J. Phys. Chem.* **93**, 3068–3077.
Jokic, A., Cutler, J. N., Anderson, D. W. & Walley, F. L. (2004). *Can. J. Soil Sci.* **84**, 291–293.
Jokic, A., Schulten, H. R., Cutler, J. N. & Schnitzer, M. (2004). *Geochim. Cosmochim. Acta*, **67**, 2585–2597.
Kelemen, S. R., Afeworki, M., Gorbaty, M. L., Kwiatek, P. J., Solum, M. S., Hu, J. Z. & Pugmire, R. J. (2002). *Energy Fuels*, **16**, 1507–1515.
Kelemen, S. R., Gorbaty, M. L. & Kwiatek, P. J. (1994). *Energy Fuels*, **8**, 896–906.
Knicker, H. (2000). *J. Environ. Qual.* **29**, 715–723.
Knicker, H., Fründ, R. & Lüdemann, H.-D. (1993). *Naturwissenschaften*, **80**, 219–221.
Knicker, H., Gonzalez-Vila, F. J., Polvillo, O., Gonzalez, J. A. & Almendros, G. (2005). *Soil Biol. Biochem.* **37**, 701–718.
Leinweber, P. & Schulten, H.-R. (1998). *Soil Sci. Soc. Am. J.* **62**, 383–393.
Mitra-Kirtley, S., Mullins, O. C., Chen, J., van Elp, J., George, S. J., Chen, C. T., O'Halloran, T. & Cramer, S. P. (1992). *Biochim. Biophys. Acta*, **1132**, 249–254.
Mitra-Kirtley, S., Mullins, O., van Elp, J., George, S. J., Chen, J. & Cramer, S. P. (1993). *J. Am. Chem. Soc.* **115**, 252–258.
Mullins, O. C., Mitra-Kirtley, S., van Elp, J. & Cramer, S. P. (1993). *Appl. Spectrosc.* **47**, 1268–1275.
Pavlychev, A. A., Hallmeier, K. H., Hennig, C., Hennig, L. & Szargan, R. (1995). *Chem. Phys.* **201**, 547–555.
Pedras, M. S. C., Jha, M. & Ahiahonu, P. W. K. (2003). *Curr. Org. Chem.* **7**, 1635–1647.
Ravel, B. & Newville, M. (2005). *J. Synchrotron Rad.* **12**, 537–541.
Ray, S. C., Pao, C. W., Chiou, J. W., Tasi, H. M., Jan, J. C. & Pong, W. F. (2005). *J. Appl. Phys.* **98**, 033708.
Regier, T., Krochak, J., Sham, T. K., Hu, Y. F., Thompson, J. & Blyth, R. I. R. (2007). *Nucl. Instrum. Methods A.* In the press.
Regier, T., Paulsen, J., Wright, G., Coulthard, I., Tan, K., Sham, T. K. & Blyth, R. I. R. (2006). *AIP Conf. Proc.* **879**, 473–476.
Rodrigues, F., do Nascimento, G. M. & Santos, P. S. (2007). *J. Electron Spectrosc. Relat. Phenom.* **155**, 148–154.
Samuel, N. T., Lee, C.-Y., Gamble, L., Fischer, D. A. & Castner, D. G. (2006). *J. Electron Spectrosc. Relat. Phenom.* **152**, 134–142.
Schulten, H.-R. & Schnitzer, M. (1997). *Biol. Fertil. Soils*, **26**, 1–15.
Schulten, H.-R., Sorge-Lewin, C. & Schnitzer, M. (1997). *Biol. Fertil. Soils*, **24**, 249–254.
Schulze, D. G. & Bertsch, P. M. (1995). *Adv. Agron.* **55**, 1–66.
Schwarzkopf, O., Borchert, M., Eggenstein, F., Flechsieg, U., Kalus, C., Lammert, H., Menthel, U., Pietsch, M., Reicherdt, G., Rotter, P., Senf, F., Zeschke, T. & Peatman, W. B. (1999). *J. Electron Spectrosc. Relat. Phenom.* **100–103**, 997–1001.
Sjöberg, G., Knicker, H., Nilsson, S. I. & Berggern, D. (2004). *Soil Biol. Biochem.* **36**, 609–618.
Somei, M. & Yamada, F. (2004). *Nat. Prod. Rep.* **21**, 278–311.
Stankiewicz, B. A. (1998). *Nitrogen-Containing Macromolecules in the Bio- and Geosphere*, pp. 1–12, *ACS Symposium Series 707*, edited by B. A. Stankiewicz and P. F van Bergen. Washington: American Chemical Society.
Stevenson, F. J. (1994). *Humus Chemistry, Genesis, Composition, Reactions.* 2nd ed. New York: John Wiley and Sons.
Stevenson, F. J. & Cole, M. A. (1999). *Cycles of Soil. Carbon, Nitrogen, Phosphorus, Sulfur, Micronutrients*, 2nd ed. New York: John Wiley and Sons.
Stöhr, J. (1992). *NEXAFS Spectroscopy.* Berlin: Springer.
Vairavamurthy, A. & Wang, S. (2002). *Environ. Sci. Technol.* **36**, 3050–3056.
Watenabe, N., Morais, J. & Alves, M. C. M. (2002). *J. Phys. Chem. B*, **106**, 11102–11107.
Wilson, C. C. (1994). *J. Chem. Crystallogr.* **24**, 371–373.
Wirick, S., Flynn, G. J., Keller, L. P. & Jacobsen, C. (2005). *67th Annual Meteoritical Society Meeting*, Rio de Janeiro, Brazil. [http://www.lpi.usra.edu/meetings/metsoc2004/pdf/5092.pdf.]
Xiao, B., Boudou, J. P. & Thomas, K. M. (2005). *Langmuir*, **21**, 3400–3409.
Zhuang, S., Xu, M. & Hu, Z. (2006). *J. For. Res.* **17**, 189–192.
Zubavichus, Y., Fuchs, O., Weinhardt, L., Heske, C., Umbach, E., Denlinger, J. D. & Grunze, M. (2004). *Radiat. Res.* **161**, 346–358.
Zubavichus, Y., Shaporenko, A., Grunze, M. & Zharnikov, M. (2005). *J. Phys. Chem. A*, **105**, 6998–7000.
Zubavichus, Y., Zharnikov, M., Shaporenko, A., Fuchs, O., Weinhardt, L., Heske, C., Umbach, E., Denlinger, J. D. & Grunze, M. (2004). *J. Phys. Chem. A*, **108**, 4557–4565.